Published in final edited form as:
J Mol Cell Cardiol. 2014 September ; 74: 231–239. doi:10.1016/j.yjmcc.2014.05.017.

Enhanced Potency of Cell-based Therapy for Ischemic Tissue Repair Using an Injectable Bioactive Epitope-presenting Nanofiber Support Matrix

Jörn Tongers, MD[*,1,4], **Matthew J. Webber, PhD**[*,2], **Erin E Vaughan, PhD**[1], **Eduard Sleep, PhD**[2], **Marie-Ange Renault, PhD**[1], **Jerome G. Roncalli, MD**[1], **Ekaterina Klyachko, PhD**[1], **Tina Thorne**[1], **Yang Yu, MD, PhD**[1], **Katja-Theres Marquardt**[1,4], **Christine E. Kamide**[1], **Aiko Ito**[1], **Sol Misener**[1], **Meredith Millay**[1], **Ting Liu**[1], **Kentaro Jujo, MD**[1], **Gangjian Qin, MD PhD**[1], **Douglas W. Losordo, MD**[1], **Samuel I. Stupp, PhD**[2,3,#], and **Raj Kishore, PhD**[1,5,#]

[1]Feinberg Cardiovascular Research Institute, Feinberg School of Medicine, Northwestern University, Chicago, IL

[2]Institute for Bionanotechnology in Medicine, Department of Medicine, Northwestern University, Chicago, IL

[3]Department of Materials Science and Engineering, Department of Chemistry, Northwestern University, Evanston, IL

[4]Department of Cardiology and Angiology, Hannover Medical School, Hannover, Germany

[5]Center for Translational Medicine, Temple University School of Medicine, Philadelphia, PA

Abstract

The translation of cell-based therapies for ischemic tissue repair remains limited by several factors, including poor cell survival and limited target site retention. Advances in nanotechnology enable the development of specifically designed delivery matrices to address these limitations and thereby improve the efficacy of cell-based therapies. Given the relevance of integrin signaling for cellular homeostasis, we developed an injectable, bioactive peptide-based nanofiber matrix that presents an integrin-binding epitope derived from fibronectin, and evaluated its feasibility as a supportive artificial matrix for bone marrow-derived pro-angiogenic cells (BMPAC) used as a therapy in ischemic tissue repair. Incubation of BMPACs with these peptide nanofibers *in vitro* significantly attenuated apoptosis while enhancing proliferation and adhesion. Pro-angiogenic

[#]Corresponding authors: Dr. Raj Kishore, PhD, Center for Translational Medicine, Department of Pharmacology, Temple University School of Medicine, MERB-953, 3500 N Broad Street, Philadelphia, PA 19140, Phone: 215-707-2523, FAX: 215-707-9890, Raj.kishore@temple.edu. Prof. Samuel I. Stupp, PhD, Northwestern University, Cook Hall, Room 1127, 2220 Campus Drive, Evanston, IL 60208, USA, Phone: (847)491-3002, Fax: (847)491-3010, s-stupp@northwestern.edu.
[*]JT and MJW contributed equally to this work

Disclosures
The authors report no conflicts of interest.

function was enhanced, as cells readily formed tubes. These effects were, in part, mediated via p38, and p44/p42 MAP kinases, which are downstream pathways of focal adhesion kinase. In a murine model of hind limb ischemia, an intramuscular injection of BMPACs within this bioactive peptide nanofiber matrix resulted in greater retention of cells, enhanced capillary density, increased limb perfusion, reduced necrosis/amputation, and preserved function of the ischemic limb compared to treatment with cells alone. This self-assembling, bioactive peptide nanofiber matrix presenting an integrin-binding domain of fibronectin improves regenerative efficacy of cell-based strategies in ischemic tissue by enhancing cell survival, retention, and reparative functions.

Keywords

microcirculation; biomaterials; nanomedicine; regenerative medicine; angiogenesis; cell therapy

Introduction

To combat the rising burden of ischemic cardiovascular disease [1], including myocardial and critical limb ischemia (CLI), new regenerative strategies must be explored. While endogenous repair mechanisms have been described, the preponderance of evidence indicates a limited capacity for self-repair in the cardiovascular system. Early clinical trials have suggested that the therapeutic application of adult stem and progenitor cells derived from the bone marrow may improve the repair and function of ischemic tissue following acute myocardial infarction [2–4], chronic myocardial ischemia [5], and CLI [6, 7). Cumulatively, these findings support the consideration of cell-based therapies as a treatment modality for ischemic cardiovascular disease [8]. However, the excitement from these early clinical studies has been tempered by uncertainties and practical limitations that have been encountered in the translation of cell-based therapy [9].

Evidence from preclinical tracking studies suggests that the majority of transplanted cells do not remain at the site of injury for more than a few hours following injection [10, 11]. In patients, only ~2% of unselected bone marrow-derived mononuclear cells and 14–39% of CD34-enriched progenitor cells remain in the myocardium one hour following intracoronary infusion, while the remainder localize to the spleen and liver [12, 13]. A further reduction in the number of detectable cells is observed over the following 3–4 days [14]. The disease microenvironment, characterized by ischemia, acidosis, oxidative stress, and inflammation, likely contributes significantly to reduced viability and retention of transplanted cells. This is particularly problematic for autologous cell-therapy in older patients with severe cardiovascular disease and associated co-morbidities, as stem and progenitor cells isolated from these patients are reduced in number, prone to apoptosis, and show impaired functionality [15–17]. Cells are also altered during isolation through detachment from native extracellular matrix (ECM), which can trigger anoikis and compromise viability and therapeutic potential. Cumulatively, the number of viable cells immediately following transplant ranges from ~30% to merely 1%, with further decline over the next 7 days following application [18, 19]. Additionally, the effects of cell-based therapies appear to be dose-dependent, with more transplanted cells resulting in a more robust therapeutic effect

[20]. Taken together with the given challenges, this suggests strategies that improve viability, retention, and bioactivity of applied stem and progenitor cells could serve to overcome some of these obstacles in order to exploit the full regenerative potential of cell-based therapies to treat ischemic tissue repair including CLI.

The design of bioactive biomaterials for cell delivery could be important in improving efficacy of cell-based therapies [21–23]. In this context, a material would provide a microenvironment for cells resembling native tissue mechanics and architecture, facilitate cell-matrix interactions, and actively support cellular homeostasis through functional signaling. A class of bioactive materials composed of nanofibers that emulate extracellular matrix architecture has been developed based on synthetic self-assembling molecules known as peptide amphiphiles (PA) [24–25]. Preclinical efforts in a variety of disease models have demonstrated that this class of materials could have broad application to regenerative medicine [26–28] although their use to enhance stem cell retention and function in ischemic tissue repair models is not yet reported.

The molecules that form these bioactive materials consist of a hydrophobic alkyl segment attached to a customizable oligopeptide (Figure 1). This amphiphilic molecular design guides self-assembly into nanofibers in aqueous environments. The filamentous architecture and mechanical properties can be controlled through the use of peptide sequences that form β-sheet hydrogen bonds, while bioactive sequences can be inserted at the terminal end of the peptide for display at high density on the nanofiber surface and can facilitate interaction with soluble proteins, receptors, and biopolymers, thus enabling the creation of an active signaling niche for cells [29–32]. The filamentous nanofibers can form three-dimensional gels upon electrostatic screening of their charged residues by electrolytes in physiologic fluids. Therefore, a viscous solution of PA nanofibers can be combined with cells and delivered via syringe injection for gelation *in situ*, obviating surgical implantation and minimizing associated tissue damage. The assembly and composition of PA molecules facilitate biodegradation into natural amino acids and lipids over weeks following injection [33]. In native ECM, integrin-matrix interactions enable a cell to communicate with its environment and help to promote cellular homeostasis and functionality [34]. One important ECM protein involved in cell-matrix interaction is fibronectin, which signals through integrins to control cellular functions that are important in the context of cell-based therapy, such as adhesion, survival, proliferation, and motility. Interestingly, fibronectin adhesion to integrins can be recreated using only a short segment of the whole protein, the Arg-Gly-Asp-Ser (RGDS) peptide [35]. Here we report that RGDS- PA nanofibers presenting this integrin-binding epitope facilitate improved efficacy of cell-based therapy in a murine model of hind limb ischemia. This represents a novel application of PA nanofiber technology to augment cell-based therapy.

Materials and Methods

Preparation of peptide amphiphiles

PAs used in these studies were prepared identically to those reported previously [30]. Nanofiber composition consisted of 100% of a diluent sequence C16–V3A3E3 (diluent PA) or a binary mixture consisting of 90% of this same diluent with 10% C16–V3A3K3RGDS

(RGDS-PA), based on the optimal ratio for this system [30]. A scrambled epitope control, C16–V3A3K3DGSR (DGSR-PA), was used at this same ratio with the diluent PA.

Cell culture

Bone marrow-derived proangiogenic cells (BMPAC) were grown from the bone marrow mononuclear cell (BMNC) fraction that was harvested from 8-week old male FVB/N wild type mice, with approval from Northwestern University ACUC. These BMPAC are phenotypically and functionally akin to mouse bone marrow derived endothelial progenitor cells and have been widely published. Given the uncertainty over exact definition of mouse EPCs, we preferred to call these cells as BMPAC. Total bone marrow was isolated and the mononuclear cell fraction was obtained by density gradient centrifugation using histopaque (Sigma). After incubation for 2 hours on uncoated cultures dishes (Nunc), non-adherent BMNC were plated on fibronectin-coated (Sigma) culture dishes and cultured in complete endothelial cell growth media (EBM-2 media, with EGM-2 MV SingleQuot, Lonza) to enrich for cells with endothelial character. On day 4, media was changed to remove non-adherent cells. BMPACs were used for experiments on day 7. Human $CD34^+$ cells from healthy donors were provided courtesy of Baxter Healthcare (Deerfield, IL). After thawing, $CD34^+$ cells were suspended in IMDM media supplemented with 10% FBS, 20 Kunitz/ml DNAseI (Sigma), and 100 U/ml streptomycin/penicillin. Prior to application, viability was assessed by trypan blue exclusion (always ≥95%) and then cells were resuspended in PBS with 0.1% BSA, with or without RGDS-PA.

Functional in vitro assays

For the following *in vitro* assays, a soluble concentration of 0.2 w/v% of PA nanofibers in media was used. All experiments were repeated at least three times. Cell viability was assessed using an MTS Assay (Promega) using 5×10^3 cells/well in 96-well plates. Cells were treated for 24 hours with the various PAs or media only, following which conversion of the MTS substrate was measured after 4 hours in triplicate per condition by absorbance at 490 nm (background 650 nm). Apoptosis was evaluated by plating BMPACs in 4-chamber slides at 5×10^4 cells/chamber and inducing apoptosis through treatment with H_2O_2 (50 μM), following which cells were assayed by microscopy in 3 independent high-power fields (20x) per condition after TUNEL staining using the Fluorescein In Situ Cell Death Detection Kit (Roche). For adhesion assays, cells were pre-treated with PA or media for 48 hours on temperature-sensitive cell culture plates (Nunc) to preserve cell surface proteins. Pretreated cells were then added to 96-well plates (2.5×10^3/well) coated with collagen type-1, laminin, or vitronectin, in addition to an uncoated surface. After 1 hour, the surface was washed and adherent cells were fixed and stained with DAPI for quantification using fluorescent microscopy in 5 high-power fields at 20x. To assess tube formation, 3×10^4 serum-starved cells were seeded per well in a 48-well plate coated with growth-factor-reduced Matrigel (BD Biosciences). The mean tube length and total number of tube-like forms were quantified by bright-field microscopy.

Quantitative real-time reverse transcriptase-polymerase chain reaction (RT-PCR)

RNA was isolated from cells with RNA STAT-60 (TEL-TEST Electronics Labs, Inc.) according to the manufacturer's instructions. Total RNA was reverse transcribed with a Taqman cDNA Synthesis Kit (Applied Biosystems) and amplified using a Taqman 7500 analyzer (Applied Biosystems). The relative expression of each mRNA was calculated by the comparative threshold cycle (CT) method and normalized to 18S expression.

Immunoblotting

Protein concentrations from cell lysate were determined by a Bradford assay, and equal protein amounts were loaded. Following standard SDS PAGE using 10% Tris-HCl SDS gels (Bio-Rad), phosphorylation of Akt and mitogen-activated protein kinase (MAPK) ERK 1/2 (p44/42) were detected using anti-Akt, anti-phospho-Akt, anti-p44/p42, and anti-phospho-p44/p42 antibodies (all 1:1000, Cell signaling). Membranes were developed via horseradish peroxidase-coupled secondary antibodies (1:2000, Bio-Rad) and enhanced chemiluminescence (SuperSignal West Pico Chemiluminescent Substrate kit, Thermo Scientific). Protein phosphorylation levels are given as the ratio of phosphorylated to total protein.

Scanning electron microscopy

Scanning electron microscopy (SEM) was performed using a S4800 scanning electron microscope with a 3 kV accelerating voltage (Hitachi). Samples of cells on coverslips were fixed with glutaraldehyde, sequentially dehydrated in ethanol, critical point dried, and coated with osmium tetraoxide.

Animals

For cell isolation and hind-limb ischemia (HLI) studies, 8-week old male FVB/N wild type mice (Charles-River) were used. For HLI studies using $hCD34^+$ cells, 8–10 week old male BALB/c nude mice (Charles-River) were used. For bioluminescence studies, hemizygous male FVB/N-Tg(β-Actin-luc)-Xen transgenic mice (Xenogen) with a modified firefly luciferase gene under the constitutive murine β-Actin promoter were used. For hind limb ischemia studies, 15 mice per group were planned. Following triage of outliers and removal of animals with severe ischemia over the course of the study, each time point includes an average of between 7–13 mice per group. For similar reasons, bioluminescence imaging studies included 4–10 animals per group per time point. All animal studies were approved by the Northwestern University Animal Care and Use Committee.

Hind-limb ischemia, laser Doppler imaging, and functional limb assessment

For the HLI model [36], mice were anesthetized with isoflurane. Using a dissecting microscope, the femoral nerve was separated from the vessel bundle. The femoral artery was ligated and excised including all superficial and deep branches. Immediately after the procedure, laser Doppler perfusion imaging (LDPI, MoorLDI-SIM System, Moor Instruments) at a wavelength of 785 nm was performed to ensure ischemia, indicated by a ratio of ischemic/non-ischemic limb of ≤0.20. At postoperative day 3, outliers with low ischemia (ratio ischemic/non-ischemic ≥0.30) or extreme ischemia (ratio ≤0.10, or

macroscopic evaluation revealing necrotic demarcation of entire limb) were removed from the study to reduce intrinsic model variability. Blood flow recovery was assessed by sequential LDPI on days 7, 14, 21 and 28 in the FVB model and days 7, 14 and 35 in the BALB/c model to determine the ratio of perfusion in the ischemic/non-ischemic limbs. To adjust for necrotic tissue loss, the mean blood flow below the inguinal ligament was multiplied by the corresponding area for each limb. LDPI was conducted on a 37°C heating pad to minimize effects associated with body temperature. Structural and functional limb recovery was classified based on clinical observation and semi-quantitative scoring. With a modified scoring system to classify limb salvage [37], tissue damage in the ischemic limb was graded according to the following scale: full recovery (grade 6); minor necrosis or nail loss (grade 5); partial toe amputation (grade 4); total toe amputation (grade 3); partial/total foot amputation (grade 2); or partial/total limb amputation (grade 1). In addition, limb motor function was scored according to the following scale: unrestricted (grade 5); no active use of toe(s)/toe spreading (grade 4); restricted foot use (grade 3); no use of foot/limb use only (grade 2); or no use of limb (grade 1) [37].

Therapeutic application of cells with PA nanofibers

For BMPAC studies, following triage of outliers at day 3, the remaining mice were randomized and treated with a single transcutaneous intramuscular injection (25 μl) into the gastrocnemius muscle of a cell dose (1×10^5) of syngeneic BMPACs [38]. Cells were either injected alone in a saline vehicle, or within a viscous 1.3 w/v% PA. For $hCD34^+$ cells, mice were similarly treated by a single transcutaneous intramuscular injection (25 μl) of 2.5×10^4 cells with or without RGDS-PA.

Histology

At postoperative day 28, the gastrocnemius was harvested, fixed in methanol, paraffin-embedded, and cross-sectioned (6μm) for histological evaluation. Sections were blocked with 10% donkey serum. Primary antibodies were diluted in PBS containing BSA. Sections were stained for CD31 using a rat anti-CD31 antibody (BD) and smooth-muscle α-actin (αSMA) using a rabbit anti-αSMA antibody (Sigma). For immunofluorescent detection, AlexaFluor-conjugated secondary antibodies were used (Invitrogen). Nuclei were stained with DAPI (Research Organics). Using fluorescent microscopy (Zeiss), $CD31^+$ capillary forms and $CD31^+/\alpha SMA^+$ arterioles were quantified in 3 distinct high-power fields (20x) from 3 independent sections in each animal.

In vivo bioluminescent imaging

For noninvasive bioluminescent imaging (BLI) of β-actin-luc^+ BMPAC, mice were anesthetized with isoflurane and placed onto a heated stage within the IVIS 100 imaging system (Xenogen). Following intraperitoneal injection (100 mg/kg) of D-luciferin potassium salt (Regis Technologies), photon emission was measured every 2 minutes from the time of injection until peak signal (Living Image 2.50.1 software, Xenogen). All images were acquired with an acquisition time of 1 minute in a 20 cm field of view with constant binning. Detected photons in pseudocolor were overlayed on grayscale light images for localization. Luminescence was quantified as the sum of all detected photons per second within a constant region of interest using Igor Pro 4.09A image analysis software (WaveMetrics),

with subtraction of background signal. Results are given as relative change from baseline over time [39].

Statistical analysis

Results were analyzed by means of StatView statistical software (SAS) or Graphpad Prism 5 (GraphPad Software). Unless otherwise indicated, data are shown as mean±SEM. After ensuring data passed normality testing (Kolmolgorov-Smirnov), differences between experimental groups were analyzed by one-way ANOVA followed by Bonferroni *post hoc* test or two way repeated-measures ANOVA followed by Bonferroni *post-hoc* test. A two-tailed P value of <0.05 was considered statistically significant.

Results

Bioactive PA nanofibers enhance therapeutically relevant function of BMPACs in vitro

Preliminary studies determined that *in vitro* assays on BMPACs were technically feasible at sub-gelation concentrations of PA nanofibers, preventing confounding effects that arise from PA-associated viscosity. SEM studies verified that cells cultured under these conditions were clearly exposed to PA nanofibers on their surface and on the cell culture substrate (Figure 2A). Cell functions that are particularly relevant to improving efficacy for cell-based therapies, including protection from apoptosis, enhanced proliferation, and increased cell adhesion, were favorably modulated *in vitro* by the addition of RGDS-PA, while controls of diluent-PA and a scrambled epitope DGSR-PA did not demonstrate a similar effect (Figure 2B–D). Incubation of BMPACs with RGDS-PA protected cells from H_2O_2-induced apoptosis ($TUNEL^+/TUNEL^-$ ratio: control 0.60±0.07, RGDS-PA 0.22±0.02, diluent PA 0.38±0.04, DGSR-PA 0.37±0.03). RGDS-PA also enhanced BMPAC proliferation (control 100±0%, RGDS-PA 303±134%, diluent PA 141±6%, DGSR-PA 156±3%) and pre-treatment of the cells with RGDS-PA increased subsequent cellular adhesion to uncoated (cell number: control 46±19, RGDS-PA 130±46) and vitronectin-coated (cell number: control 38±14, RGDS-PA 146±33) surfaces.

We also assessed the impact of RGDS-PA on more complex cellular function. The regenerative function of many stem and progenitor cells has been at least partially attributable to pro-angiogenic function. Using a matrigel assay (Figure 3), RGDS-PA enhanced the total length of tube-like structures formed by BMPACs (total tube length in pixels for control vs. RGDS-PA: 6 hrs, 0±0 vs. 1340±387; day 1, 153±88 vs. 2280±571; day 3, 1033±470 vs. 2347±765; day 5, 1219±466 vs. 2563±611). Also, the total number of tube-like structures was significantly increased (total tube number for control vs. RGDS-PA: 6 hrs, 0±0 vs. 21±7; day 1, 3±2 vs. 30±7; day 3, 15±6 vs. 27±0; day 5, 15±5 vs. 28±4).

RGDS-PA nanofibers activate integrin signaling cascades

Cellular homeostasis is regulated, at least in part, through integrin signaling and is mediated via focal adhesion kinase (FAK) and several downstream cascades. Cell apoptosis and proliferation, for example, are mediated via Akt and p44/42 pathways. The treatment of BMPACs with RGDS-PA activated phosphorylation of the Akt survival pathway (Figure 4A), comparable to SDF-1, a known Akt activator (15 minutes, control 100±0%, SDF-1

581±279, RGDS-PA 319±32%; 30 minutes, control 100±0%, SDF-1 345±83%, RGDS-PA 329±87%; 60 minutes, control 100±0%, SDF-1 235±75%, RGDS-PA 135±46%). Additionally, mRNA expression levels of pro-apoptotic p53 mRNA (Figure 4C) were significantly reduced in cells treated with RGDS-PA (control 32±4, RGDS-PA 19±3). The activation of p44/42 (Figure 4B), a pro-proliferative cascade, was significantly increased following treatment with RGDS-PA, even compared to treatment with SDF-1 (15 minutes, control 100±0%, SDF-1 219±36%, RGDS-PA 1886±1062; 30 minutes, control 100±0%, SDF-1 215±80, RGDS-PA 1588±411%; 60 minutes, control 100±0%, SDF-1 203±135%, RGDS-PA 614±492%). Accordingly, RGDS-PA resulted in higher mRNA expression of downstream mitogenic targets (Figure 4D–F), specifically Ki67 (control 1.0±0, RGDS-PA 3.2±0.8), cyclin-A (control 1.0±0, RGDS-PA 4.2±1.2), and cyclin E (control 1.0±0, RGDS-PA 2.0±0.2). Functionally, FAK-mediated activation is known to promote cytoskeletal rearrangement and increased focal adhesion formation. Cells plated on RGDS-PA surfaces showed prominent phalloidin staining (Figure 4G).

Bioactive PA nanofiber matrix enhances regenerative potency of cell-based therapy in ischemic tissue repair

Based on the beneficial modulation of BMPAC function by RGDS-PA observed *in vitro*, we evaluated the regenerative potency of this combined strategy in critical limb ischemia. When compared to the same dose of cells alone, this combined approach demonstrated enhanced structural and functional recovery in the ischemic limb (Figure 5). Animals that were treated with BMPACs combined with RGDS-PA showed significantly less necrosis and fewer amputations, as evidenced by a significant improvement in limb salvage score on day 28 (Figure 5A: HLI control 2.0±0.3, BPMAC+RGDS-PA 3.8±0.3, BMPAC 2.9±0.3, RGDS-PA 2.3±0.4.). Similarly, animals treated with BMPACs in the RGDS-PA matrix had significant improvement in motor function of the ischemic limb, resulting in a greater limb motor activity score (Figure 5B: HLI control 2.2±0.3, BPMAC+RGDS-PA 3.9±0.3, BMPAC 2.9±0.2, RGDS-PA 2.6±0.4). The enhanced limb recovery was associated with improved microcirculation, demonstrated by a significant increase in the number of $CD31^+$ capillary-like structures when BMPACs were combined with RGDS-PA (Figure 5D: HLI control 56±2/hpf, BMPAC+RGDS-PA 91±5/hpf, BMPAC 72±3/hpf, RGDS-PA 61±2/hpf). Recovery of blood flow in the ischemic limb, measured by LDPI, was improved at day 28 in mice that had been treated with BMPACs and RGDS-PA (Figure 5E: ischemic/non-ischemic limb ratio: HLI control 0.34±0.04, BPMAC+RGDS-PA 0.70±0.08, BMPAC 0.53±0.02, RGDS-PA 0.47±0.03). In a proof-of-concept experiment, we assessed whether delivery with RGDS-PA resulted in increased viability and retention of BMPACs in the ischemic limb. Luciferase-expressing BMPACs were injected with our without RGDS-PA following HLI. Notably, BMPACs delivered with RGDS-PA resulted in a higher level of luminescence than BMPACs alone (Figure 5F; day 1, 102±36% vs. 167±15%; day 4, 106±40% vs. 971±215%; day 7, 132±50 vs. 692±141%; day 28, -2±-1% vs. -6±3%). This suggests that cell delivery supported by the RGDS-PA matrix enhances the number of viable cells within ischemic tissue, which may be due to reduced apoptosis, enhanced proliferation, and/or improved retention, consistent with our *in vitro* findings. The versatility of this matrix was also established as a delivery strategy for human-derived $CD34^+$ cells (see online supplement

and Figure S1). Its biocompatibility and tissue stability was also assessed (see online supplement and Figure S2).

Discussion

Clinical evidence has supported some efficacy for cell-based therapies in ischemic tissue repair, but practical limitations, including poor cell viability and retention, have prevented their full regenerative potency from being realized. The use of specifically engineered biomaterials to support therapeutic stem and progenitor cells is a potential strategy to improve cell-based therapies. Here, we demonstrate that a peptide-based nanofiber matrix presenting the integrin-binding domain from fibronectin favorably modulates apoptosis, proliferation, adhesion, and tube formation of cultured BMPACs. When identical doses of BMPACs or $hCD34^+$ cells were delivered in combination with this RGDS-PA matrix, the regenerative potency of the cell-based therapy was enhanced in an animal model of ischemic tissue repair. This was attributable, in part, to an increase in the number of viable cells within the therapeutic target zone for the case where cells were delivered with RGDS-PA.

An ideal biomaterial for cell-based therapy in cardiovascular disease should provide a bioactive three-dimensional microenvironment that resembles the architecture and function of native ECM [21]. Such a material would be designed with optimal mechanical properties, present biological signals that improve cell function, degrade at a controlled rate into harmless metabolites, elicit a minimal inflammatory response, and be applied through a minimally invasive route. The PA nanofiber platform described has the ability to meet these criteria, and could be further modified and optimized for enhanced stem and progenitor cell support. Through molecular design, the type, number, and density of biological signals presented on the nanofiber surface could be modified for improved bioactive signaling [40], or multiple bioactive or matrix-derived signals could be combined within one nanofiber [41], An example of particular relevance for ischemic tissue repair could explore epitopes that mimic VEGF to support enhanced pro-angiogenic function in cell-based therapies [32], It is increasingly appreciated that mechanical properties of a biomaterial can play a role in directing cell function or lineage [42]. Along these lines, the stiffness of PA nanofibers can be also tuned through molecular design [43], suggesting that efforts to tailor mechanical properties of PA nanofibers for a specific therapeutic cell type could be a strategy to further improve cell-based regenerative functions. In terms of translational potential, the immune response is a crucial criteria affecting future implementation [44]. The present study suggests that this synthetic matrix does not elicit a notable local or systemic immune response. More rigorous toxicology and biodistribution studies must be performed prior to clinical implementation, but these early pre-clinical findings are promising. The PA nanofibers here were also designed to gel once introduced within tissue, allowing for facile transcutaneous injection for delivery with cells. It is foreseeable that this minimally invasive delivery approach could extend to catheter application.

This proof-of-concept study demonstrates a potential role for bioactive matrices to exploit the full regenerative potential of cell-based therapies in ischemic tissue repair. However, future work must thoroughly evaluate and optimize several aspects of this strategy prior to clinical translation. Understanding the biological importance of structural characteristics in

these biomaterials, such as epitope density and nanofiber geometry, are interesting questions to evaluate further. We hypothesize that these parameters may be important in optimizing cell-matrix interactions, and can thus affect efficacy. The specific features of an optimal material likely depend on the underlying pathology along with considerations for the specific tissue or organ to be treated. Also, the importance of material stability, degradation, and persistence need to be optimized in the context of the particular dynamics and kinetics of the therapeutic target. For example, our present results from histological tracking suggest that ischemic tissue may present a harsher, more protease-rich milieu that is detrimental to persistence of peptide-based materials. Notably, the time-course of RGDS-PA persistence coincided with that for retention of BMPACs in the ischemic limb, assessed by *in vivo* imaging. Therefore, efforts to modify the PA sequence to produce more degradation-resistant nanofibers may afford prolonged retention of injected cells, and in turn improve therapeutic efficacy. Finally, the clearance, metabolism, and pharmacokinetics of the degradation products must be further elucidated in order to be confident that no toxicity arises from the application of these materials or their degradation products.

Insights from clinical trials have raised questions about the extent of regeneration that may be possible from a single dose of stem or progenitor cells. In light of some of the concerns surrounding cell retention and function in diseased tissue, it appears that more sophisticated and multi-faceted strategies are needed to improve efficacy [9]. The present study constitutes a step in this direction, and the versatility of PA-based materials in preparing bioactive matrices could be further leveraged to prepare a more sophisticated approach. We would envision that in the regeneration of tissue for cardiovascular pathologies, an approach that combines various stem, progenitor or stromal cells with paracrine factors and matrix-derived signaling elements would improve the potency of cell-based strategies for ischemic tissue repair.

Conclusions

Cell-based therapies have been extensively explored as a treatment for myocardial and peripheral ischemia, but challenges associated with cell retention and survival may limit efficacy. Self-assembling bioactive peptide nanofibers presenting the integrin-binding domain of fibronectin support cell function and, thereby, enhance the therapeutic potency of cell-based strategies for ischemic tissue repair. This approach, employing a specifically designed nanofiber matrix in combination with therapeutic cell populations, is a promising strategy to combat certain limitations encountered in the translation of cell-based therapies.

Supplementary Material

Refer to Web version on PubMed Central for supplementary material.

Acknowledgments

This work was supported in part by funding from the National Institute of Health, specifically grants HL091983, HL105597, HL095874, HL053354, HL108795 and EB003806. JT was supported by the American Heart Association and the German Heart Foundation. ES was supported by the IBNAM-Baxter Early Career Development Award, and this project was funded by an IBNAM-Baxter Research Incubator grant and a Dixon

Translational Research Award. We thank Xiaomin Zhang and Dixon B. Kaufman, formerly from the department of Transplant Surgery at Northwestern Memorial Hospital, for technical support with bioluminescent imaging.

References

1. Go AS, Mozaffarian D, Roger VL, Benjamin EJ, Berry JD, Borden WB, et al. Heart disease and stroke statistics--2013 update: a report from the American Heart Association. Circulation. 2013; 127(1):e6–e245. [PubMed: 23239837]
2. Abdel-Latif A, Bolli R, Tleyjeh IM, Montori VM, Perin EC, Hornung CA, et al. Adult Bone Marrow-Derived Cells for Cardiac Repair: A Systematic Review and Meta-analysis. Arch Intern Med. 2007; 167(10):989–97. [PubMed: 17533201]
3. Lipinski MJ, Biondi-Zoccai GG, Abbate A, Khianey R, Sheiban I, Bartunek J, et al. Impact of intracoronary cell therapy on left ventricular function in the setting of acute myocardial infarction: a collaborative systematic review and meta-analysis of controlled clinical trials. J Am Coll Cardiol. 2007; 50(18):1761–7. [PubMed: 17964040]
4. Martin-Rendon E, Brunskill SJ, Hyde CJ, Stanworth SJ, Mathur A, Watt SM. Autologous bone marrow stem cells to treat acute myocardial infarction: a systematic review. Eur Heart J. 2008; 29(15):1807–18. [PubMed: 18523058]
5. Losordo DW, Henry TD, Davidson C, Sup Lee J, Costa MA, Bass T, et al. Intramyocardial, autologous CD34+ cell therapy for refractory angina. Circ Res. 2011; 109(4):428–36. [PubMed: 21737787]
6. Tateishi-Yuyama E, Matsubara H, Murohara T, Ikeda U, Shintani S, Masaki H, et al. Therapeutic angiogenesis for patients with limb ischaemia by autologous transplantation of bone-marrow cells: a pilot study and a randomised controlled trial. Lancet. 2002; 360(9331):427–35. [PubMed: 12241713]
7. Fujita Y, Kinoshita M, Furukawa Y, Nagano T, Hashimoto H, Hirami Y, et al. Phase II clinical trial of CD34+ cell therapy to explore endpoint selection and timing in patients with critical limb ischemia. Circ J. 2014; 78(92):490–501. [PubMed: 24257136]
8. Bartunek J, Dimmeler S, Drexler H, Fernandez-Aviles F, Galinanes M, Janssens S, et al. The consensus of the task force of the European Society of Cardiology concerning the clinical investigation of the use of autologous adult stem cells for repair of the heart. Eur Heart J. 2006; 27(11):1338–40. [PubMed: 16543252]
9. Tongers J, Losordo DW, Landmesser U. Stem and progenitor cell-based therapy in ischaemic heart disease: promise, uncertainties, and challenges. Eur Heart J. 2011; 32(10):1197–206. [PubMed: 21362705]
10. Aicher A, Brenner W, Zuhayra M, Badorff C, Massoudi S, Assmus B, et al. Assessment of the tissue distribution of transplanted human endothelial progenitor cells by radioactive labeling. Circulation. 2003; 107(16):2134–9. [PubMed: 12695305]
11. Brenner W, Aicher A, Eckey T, Massoudi S, Zuhayra M, Koehl U, et al. 111In-labeled CD34+ hematopoietic progenitor cells in a rat myocardial infarction model. J Nucl Med. 2004; 45(3):512–8. [PubMed: 15001696]
12. Hofmann M, Wollert KC, Meyer GP, Menke A, Arseniev L, Hertenstein B, et al. Monitoring of bone marrow cell homing into the infarcted human myocardium. Circulation. 2005; 111(17):2198–202. [PubMed: 15851598]
13. Dedobbeleer C, Blocklet D, Toungouz M, Lambermont M, Unger P, Degaute JP, et al. Myocardial homing and coronary endothelial function after autologous blood CD34+ progenitor cells intracoronary injection in the chronic phase of myocardial infarction. J Cardiovasc Pharmacol. 2009; 53(6):480–5. [PubMed: 19433985]
14. Schachinger V, Aicher A, Dobert N, Rover R, Diener J, Fichtlscherer S, et al. Pilot trial on determinants of progenitor cell recruitment to the infarcted human myocardium. Circulation. 2008; 118(14):1425–32. [PubMed: 18794392]
15. Hill JM, Zalos G, Halcox JP, Schenke WH, Waclawiw MA, Quyyumi AA, et al. Circulating endothelial progenitor cells, vascular function, and cardiovascular risk. N Engl J Med. 2003; 348(7):593–600. [PubMed: 12584367]

16. Vasa M, Fichtlscherer S, Aicher A, Adler K, Urbich C, Martin H, et al. Number and migratory activity of circulating endothelial progenitor cells inversely correlate with risk factors for coronary artery disease. Circ Res. 2001; 89(1):E1–7. [PubMed: 11440984]
17. Heeschen C, Lehmann R, Honold J, Assmus B, Aicher A, Walter DH, et al. Profoundly reduced neovascularization capacity of bone marrow mononuclear cells derived from patients with chronic ischemic heart disease. Circulation. 2004; 109(13):1615–22. [PubMed: 15037527]
18. Balsam LB, Wagers AJ, Christensen JL, Kofidis T, Weissman IL, Robbins RC. Haematopoietic stem cells adopt mature haematopoietic fates in ischaemic myocardium. Nature. 2004; 428(6983): 668–73. [PubMed: 15034594]
19. Zhang M, Methot D, Poppa V, Fujio Y, Walsh K, Murry CE. Cardiomyocyte grafting for cardiac repair: graft cell death and anti-death strategies. J Mol Cell Cardiol. 2001; 33(5):907–21. [PubMed: 11343414]
20. Assmus B, Honold J, Schachinger V, Britten MB, Fischer-Rasokat U, Lehmann R, et al. Transcoronary transplantation of progenitor cells after myocardial infarction. N Engl J Med. 2006; 355(12):1222–32. [PubMed: 16990385]
21. Mooney DJ, Vandenburgh H. Cell delivery mechanisms for tissue repair. Cell Stem Cell. 2008; 2(3):205–13. [PubMed: 18371446]
22. Segers VF, Lee RT. Biomaterials to enhance stem cell function in the heart. Circ Res. 2011; 109(8):910–22. [PubMed: 21960724]
23. Hartgerink JD, Beniash E, Stupp SI. Self-assembly and mineralization of peptide-amphiphile nanofibers. Science. 2001; 294(5547):1684–8. [PubMed: 11721046]
24. Webber MJ, Kessler JA, Stupp SI. Emerging peptide nanomedicine to regenerate tissues and organs. J Intern Med. 2010; 267(1):71–88. [PubMed: 20059645]
25. Webber MJ, Berns EJ, Stupp SI. Supramolecular Nanofibers of Peptide Amphiphiles for Medicine. Israel Journal of Chemistry. 2013; 53(8):530–54. [PubMed: 24532851]
26. Lee SS, Huang BJ, Kaltz SR, Sur S, Newcomb CJ, Stock SR, et al. Bone regeneration with low dose BMP-2 amplified by biomimetic supramolecular nanofibers within collagen scaffolds. Biomaterials. 2013; 34(2):452–9. [PubMed: 23099062]
27. Shah RN, Shah NA, Del Rosario Lim MM, Hsieh C, Nuber G, Stupp SI. Supramolecular design of self-assembling nanofibers for cartilage regeneration. Proceedings of the National Academy of Sciences of the United States of America. 2010; 107(8):3293–8. [PubMed: 20133666]
28. Tysseling-Mattiace VM, Sahni V, Niece KL, Birch D, Czeisler C, Fehlings MG, et al. Self-assembling nanofibers inhibit glial scar formation and promote axon elongation after spinal cord injury. J Neurosci. 2008; 28(14):3814–23. [PubMed: 18385339]
29. Cui H, Webber MJ, Stupp SI. Self-assembly of peptide amphiphiles: from molecules to nanostructures to biomaterials. Biopolymers. 2010; 94(1):1–18. [PubMed: 20091874]
30. Webber MJ, Tongers J, Renault MA, Roncalli JG, Losordo DW, Stupp SI. Development of bioactive peptide amphiphiles for therapeutic cell delivery. Acta biomaterialia. 2010; 6(1):3–11. [PubMed: 19635599]
31. Webber MJ, Han X, Murthy SN, Rajangam K, Stupp SI, Lomasney JW. Capturing the stem cell paracrine effect using heparin-presenting nanofibres to treat cardiovascular diseases. J Tissue Eng Regen Med. 2010; 4(8):600–10. [PubMed: 20222010]
32. Webber MJ, Tongers J, Newcomb CJ, Marquardt KT, Bauersachs J, Losordo DW, et al. Supramolecular nanostructures that mimic VEGF as a strategy for ischemic tissue repair. Proceedings of the National Academy of Sciences of the United States of America. 2011; 108(33): 13438–43. [PubMed: 21808036]
33. Ghanaati S, Webber MJ, Unger RE, Orth C, Hulvat JF, Kiehna SE, et al. Dynamic in vivo biocompatibility of angiogenic peptide amphiphile nanofibers. Biomaterials. 2009; 30(31):6202–12. [PubMed: 19683342]
34. Giancotti FG, Ruoslahti E. Integrin signaling. Science. 1999; 285(5430):1028–32. [PubMed: 10446041]
35. Pierschbacher MD, Ruoslahti E. Cell attachment activity of fibronectin can be duplicated by small synthetic fragments of the molecule. Nature. 1984; 309(5963):30–3. [PubMed: 6325925]

36. Couffinhal T, Silver M, Zheng LP, Kearney M, Witzenbichler B, Isner JM. Mouse model of angiogenesis. Am J Pathol. 1998; 152(6):1667–79. [PubMed: 9626071]
37. Heil M, Ziegelhoeffer T, Wagner S, Fernandez B, Helisch A, Martin S, et al. Collateral artery growth (arteriogenesis) after experimental arterial occlusion is impaired in mice lacking CC-chemokine receptor-2. Circ Res. 2004; 94(5):671–7. [PubMed: 14963007]
38. Tateno K, Minamino T, Toko H, Akazawa H, Shimizu N, Takeda S, et al. Critical roles of muscle-secreted angiogenic factors in therapeutic neovascularization. Circ Res. 2006; 98(9):1194–202. [PubMed: 16574905]
39. Tanaka M, Swijnenburg RJ, Gunawan F, Cao YA, Yang Y, Caffarelli AD, et al. In vivo visualization of cardiac allograft rejection and trafficking passenger leukocytes using bioluminescence imaging. Circulation. 2005; 112(9 Suppl):I105–10. [PubMed: 16159800]
40. Storrie H, Guler MO, Abu-Amara SN, Volberg T, Rao M, Geiger B, et al. Supramolecular crafting of cell adhesion. Biomaterials. 2007; 28(31):4608–18. [PubMed: 17662383]
41. Niece KL, Hartgerink JD, Donners JJ, Stupp SI. Self-assembly combining two bioactive peptide-amphiphile molecules into nanofibers by electrostatic attraction. Journal of the American Chemical Society. 2003; 125(24):7146–7. [PubMed: 12797766]
42. Discher DE, Mooney DJ, Zandstra PW. Growth factors, matrices, and forces combine and control stem cells. Science. 2009; 324(5935):1673–7. [PubMed: 19556500]
43. Pashuck ET, Cui H, Stupp SI. Tuning supramolecular rigidity of peptide fibers through molecular structure. Journal of the American Chemical Society. 2010; 132(17):6041–6. [PubMed: 20377229]
44. Anderson JM, Rodriguez A, Chang DT. Foreign body reaction to biomaterials. Semin Immunol. 2008; 20(2):86–100. [PubMed: 18162407]

Highlights

- Bone marrow mononuclear cells are clinically relevant for tissue regeneration
- Nanofiber matrix developed presenting fibronectin-derived adhesion sequence
- Matrix promotes survival, proliferation, adhesion, and angiogenic function of BMPAC
- Regenerative function in ischemic tissue enhanced with nanofiber support matrix
- Specifically designed support matrix could be a component in improved cell therapy

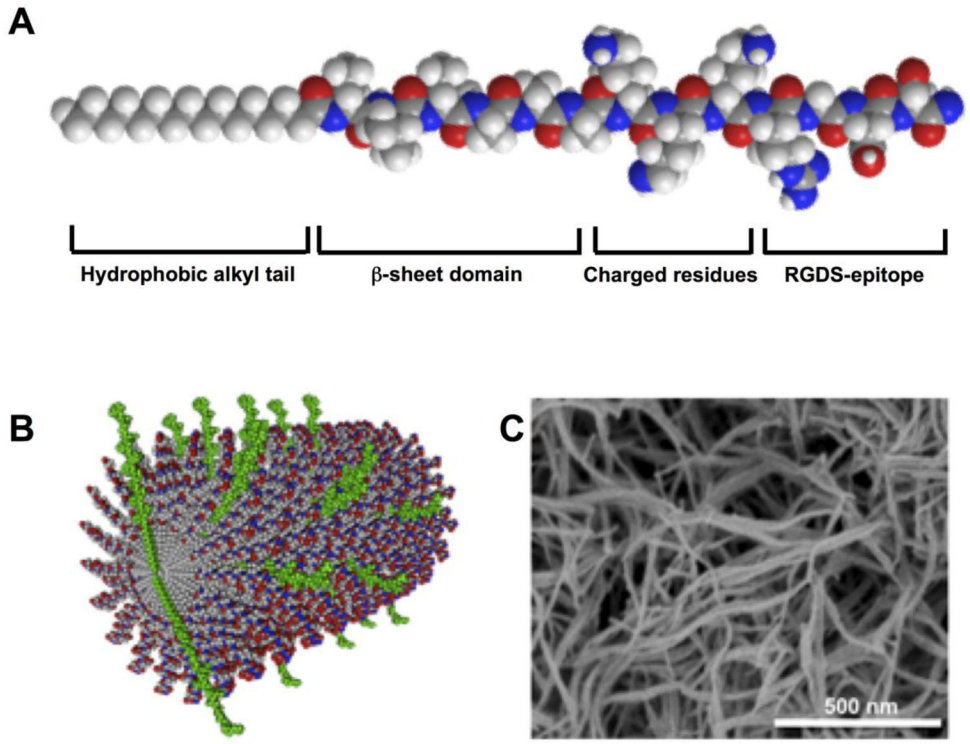

Figure 1.

(A) Molecular structure of an RGDS-PA molecule, indicating the specific design elements within the molecule. **(B)** In aqueous environments, PA molecules assemble into cylindrical nanofibers, with the RGDS-epitope-bearing molecules (green) distributed throughout the nanofiber. **(C)** Assembled nanofibers can form a three-dimensional nanofiber gel network, verified by a SEM.

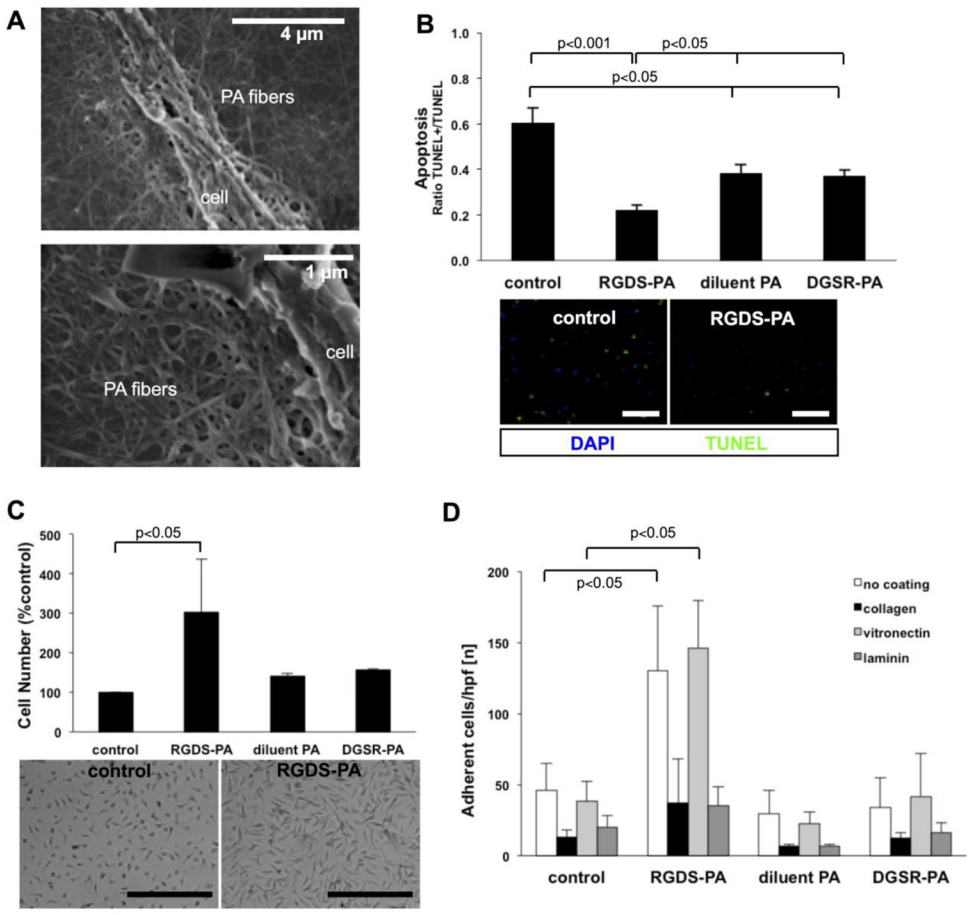

Figure 2.

(A) For *In vitro* studies of BMPACs, RGDS-PA nanofibers coat the BMPAC surface along with the surface of the culture substrate by SEM. **(B)** Apoptosis, induced in BMPACs by H_2O_2, quantified as the ratio of TUNEL+ to TUNEL- cells, n=4–10/condition. (**C**) MTS assay results showing relative BMPAC cell number, indicative of proliferation, when treated with different PAs (n=3–6/condition). (**D**) Adhesion (n=5 hpf/group) to control plastic, collagen, vitronectin and laminin for BMPACs pre-treated with different PAs. Scale bars for micrographs are 100 µm.

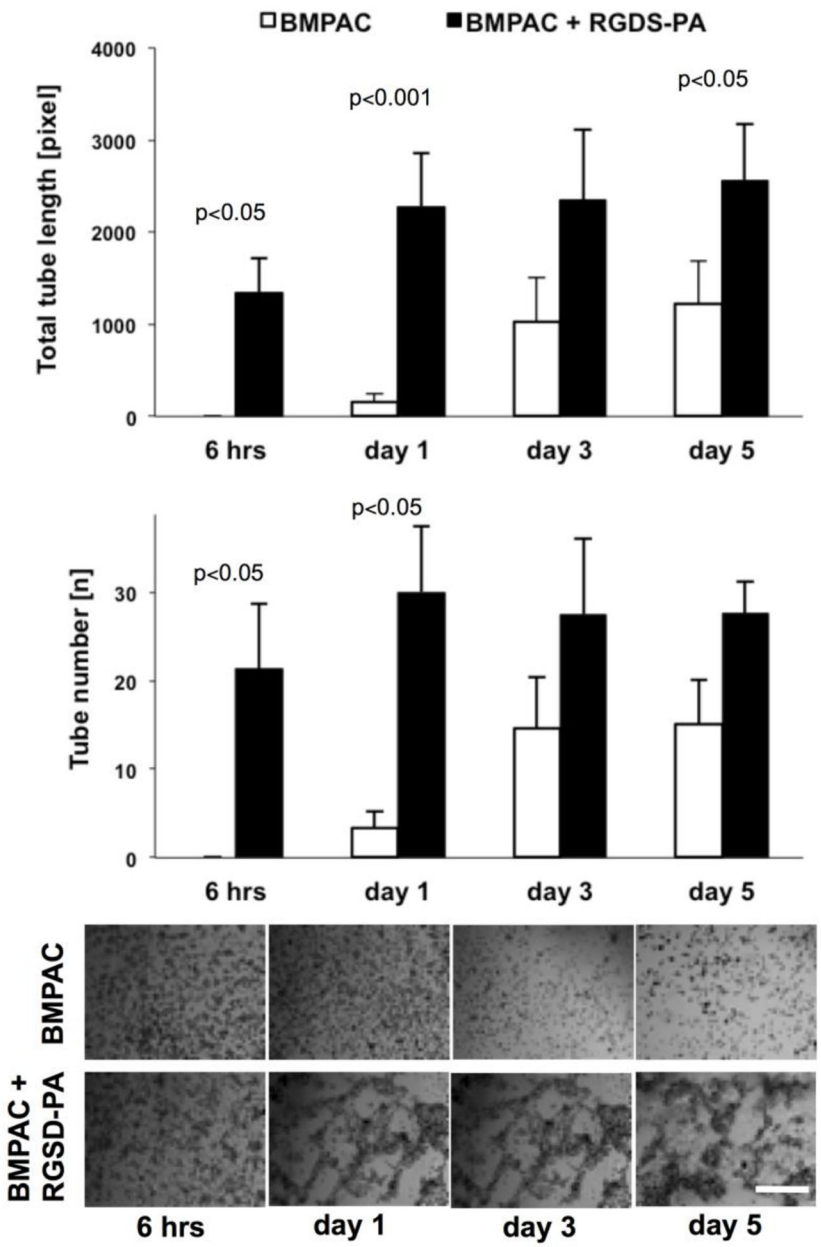

Figure 3.

A matrigel assay used to assess pro-angiogenic potential of BMPACs cultured with or without RGDS-PA (n=3–9/condition/timepoint). Scale bar shown is 100 μm for all micrographs.

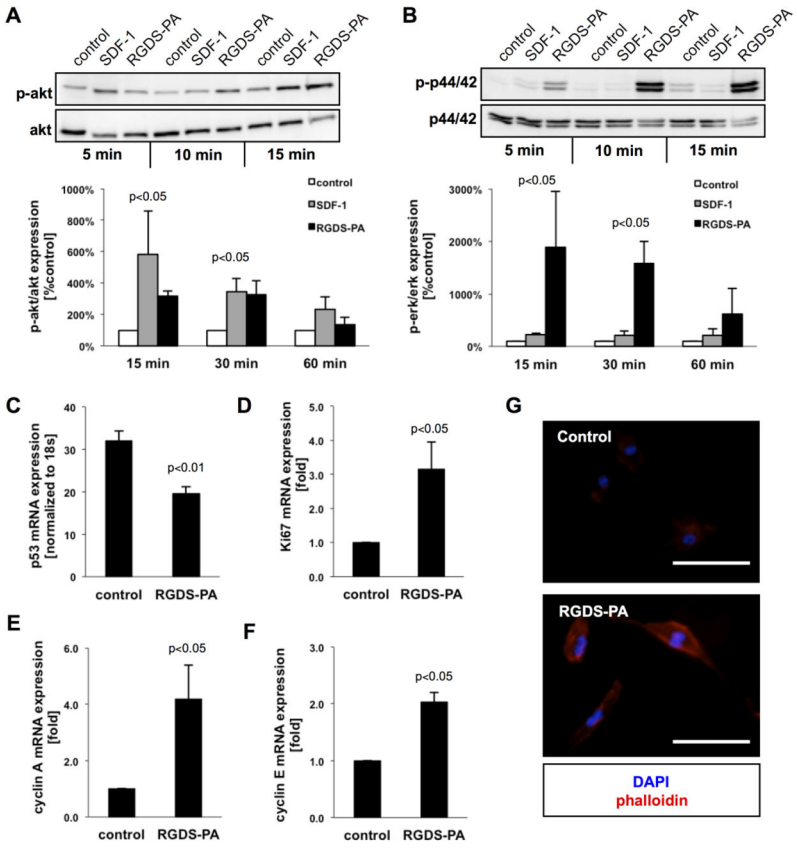

Figure 4.

(A) A representative western blot, with quantification, for the ratio of phospho-Akt to Akt in BMPACs, with SDF-1 as a positive control (n=3–4/condition/time point). **(B)** A representative western blot, with quantification, for the ratio of phospho-p44/42 to p44/42 (n=3–4/condition/time point). **(C)** mRNA expression of the pro-apoptotic marker p53. mRNA expression of mitogenic markers (**D**) Ki67, (**E**) Cyclin A, and (**F**) Cyclin E. **(G)** Phalloidin staining of BMPACs incubated on control or RGDS-PA-coated surfaces. Scale bars for micrographs are 25 μm.

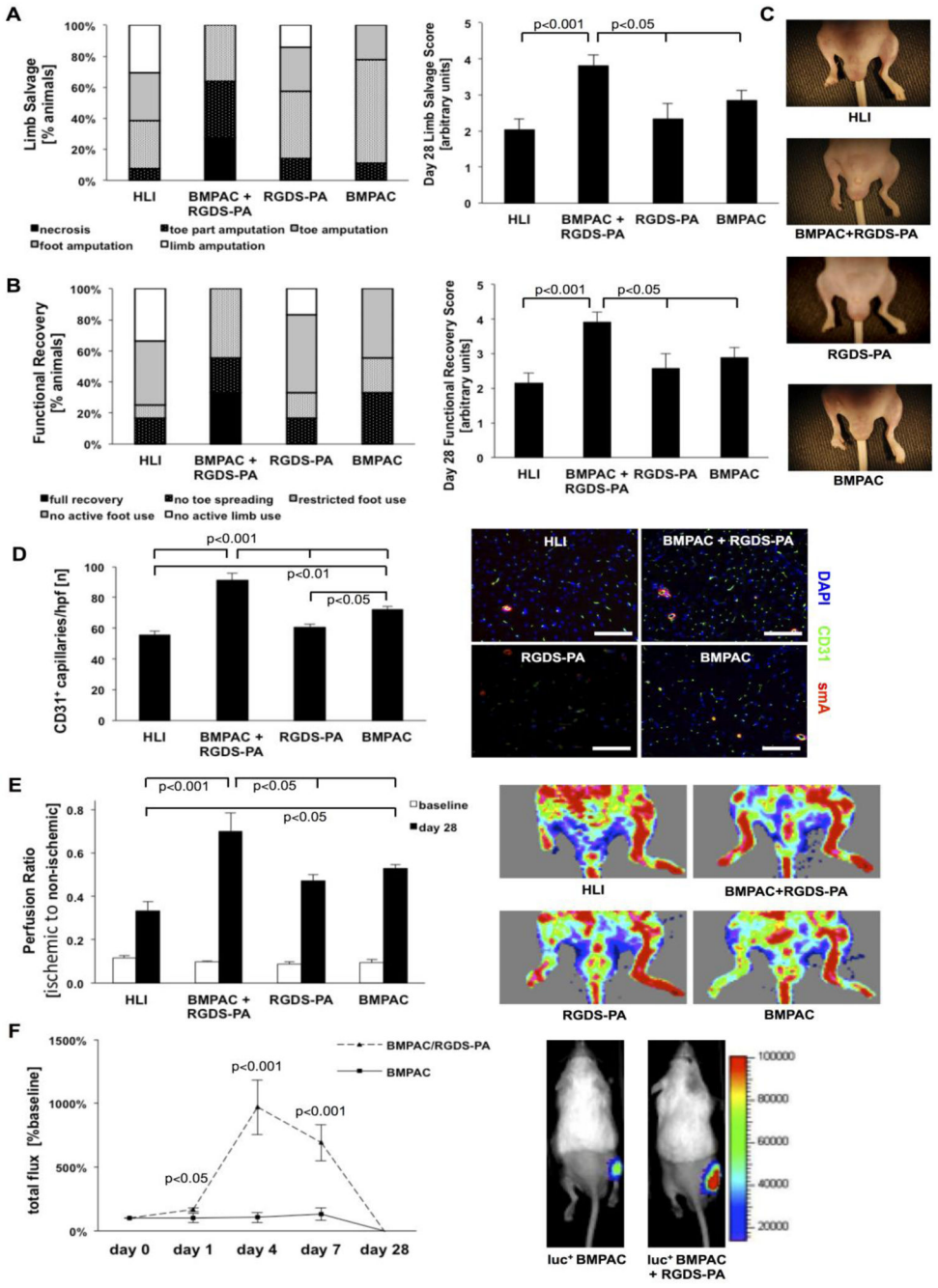

Figure 5.

In vivo evaluation of BMPACs delivered with RGDS-PA. **(A)** The percentage of mice with various grades of necrosis, along with the overall limb salvage score for each group at day 28. **(B)** The percentage of mice with various grades of motor function, along with the overall motor function score for each group at day 28. **(C)** Example gross observations of ischemia and necrosis at day 28. **(D)** Quantification of CD31+ capillaries per high powered field and representative images of CD31 and smooth muscle actin staining (n=5–9/group) with scale bars for micrographs indicating 100 μm. **(E)** Laser Doppler perfusion ratio (ischemic to non-

ischemic limb perfusion) and representative LDPI images from each group (n=7–13/group). **(F)** Measurement of bioluminescence in mice injected with β-actin-luc^{+} BMPACs with and without RGDS PA, expressed as total flux in comparison to baseline, along with representative bioluminescence images at day 7 (n=4–10/group/timepoint).